Tryptophan Fluorescence Reveals the Conformational State of a Dynamic Loop in Recombinant Porcine Fructose-1,6-bisphosphatase[†,‡]

Scott W. Nelson, Cristina V. Iancu, Jun-Yong Choe, Richard B. Honzatko, and Herbert J. Fromm*

Department of Biochemistry, Biophysics, and Molecular Biology, Iowa State University, Ames, Iowa 50011

Received March 17, 2000; Revised Manuscript Received May 30, 2000

ABSTRACT: Wild-type porcine fructose-1,6-bisphosphatase (FBPase) has no tryptophan residues. Hence, the mutation of Try57 to tryptophan places a unique fluorescent probe in the structural element (loop 52−72) putatively responsible for allosteric regulation of catalysis. On the basis of steady-state kinetics, circular dichroism spectroscopy, and X-ray crystallography, the mutation has little effect on the functional and structural properties of the enzyme. Fluorescence intensity from the Trp57 mutant is maximal in the presence of divalent cations, fructose 6-phosphate and orthophosphate, which together stabilize an R-state conformation in which loop 52−72 is engaged with the active site. The level of fluorescence emission decreases monotonically with increasing levels of AMP, an allosteric inhibitor, which promotes the T-state, disengaged-loop conformation. The titration of various metal−product complexes of the Trp57 mutant with fructose 2,6-bisphosphate ($F26P_2$) causes similar decreases in fluorescence, suggesting that $F26P_2$ and AMP individually induce similar conformational states in FBPase. Fluorescence spectra, however, are sensitive to the type of divalent cation (Zn^{2+}, Mn^{2+}, or Mg^{2+}) and suggest conformations in addition to the R-state, loop-engaged and T-state, loop-disengaged forms of FBPase. The work presented here demonstrates the utility of fluorescence spectroscopy in probing the conformational dynamics of FBPase.

Fructose-1,6-bisphosphatase [D-fructose-1,6-bisphosphate 1-phosphohydrolase, EC 3.1.3.11 (FBPase[1])] catalyzes the hydrolysis of fructose 1,6-bisphosphate ($F16P_2$) to fructose 6-phosphate (F6P) and inorganic phosphate (P_i) (*1*, *2*). FBPase, along with fructose-6-phosphate 1-kinase, defines a futile cycle in the gluconeogenic/glycolytic pathways. Hence, FBPase activity is regulated tightly, being inhibited by $F26P_2$ and AMP (*3*−*5*). The kinetic mechanism of AMP inhibition is nonlinear and noncompetitive with respect to $F16P_2$ and nonlinear and competitive with respect to Mg^{2+} (*6*, *7*). FBPase requires divalent cations (Mg^{2+}, Mn^{2+}, or Zn^{2+}), and rates of reaction vary sigmoidally with metal ion concentration (Hill coefficient of 2) (*8*−*10*). AMP binds to allosteric sites, which are 28 Å from the nearest active site (*11*). $F26P_2$ exhibits competitive inhibition kinetics with respect to $F16P_2$, and binds to the active site as a substrate analogue. AMP and $F26P_2$ inhibit FBPase synergistically (*3*−*5*). Indeed, the k_{off} for AMP decreases in the presence of $F26P_2$ (*12*).

FBPase is a homotetramer [subunit with an M_r of 37 000 (*13*)], which exists in at least two conformational states called R and T (*14*, *15*). AMP, with or without $F26P_2$, stabilizes the inactive T-state (*16*−*18*). The active R-state is favored by substrates or products in combination with metal cations (*14*, *19*). Directed mutations implicate loop 52−72 in the allosteric regulation of FBPase (*20*, *21*). Product complexes with FBPase in the presence of Mg^{2+} and Zn^{2+} reveal an ordered loop, closely associated with the active site. Product complexes with AMP, on the other hand, reveal a disordered loop, and all but one metal cation displaced from the active site (*22*). A mechanism for allosteric regulation of catalysis in FBPase, proposed by Choe et al. (*19*), involves two conformational states of loop 52−72 (called engaged and disengaged). AMP and, presumably, $F26P_2$ stabilize a disengaged loop, whereas metal cations stabilize an engaged loop.

Although crystallographic studies provide rich detail, they are difficult to perform over a broad range of experimental conditions. Furthermore, the process of crystallization selects typically only one family of closely related conformers from what might be a diverse population of conformers in solution. Hence, to complement X-ray diffraction studies, and provide information regarding FBPase conformers over a variety of experimental conditions, we have introduced a spectroscopic probe into loop 52−72. As porcine FBPase has no tryptophan residues, a directed mutation can easily introduce a unique fluorophore. Tyr57 of loop 52−72 is an attractive target for tryptophan substitution. Tyr57 has a large side chain, which exists in different environments in the engaged and disengaged conformation of loop 52−72. Reported here are the kinetic and structural properties of the Trp57 mutant of FBPase, and its conformational response, as assessed by

[†] This work was supported in part by National Institutes of Health Research Grant NS 10546 and National Science Foundation Grant MCB-9603595. This is journal paper 18896 from the Iowa Agriculture and Home Economic Experiment Station, Ames, IA, Project 3191, and is supported by Hatch Act and State of Iowa funds.

[‡] The atomic coordinates and structure factors (codes 1FJ6 and 1FJ9) have been deposited in the Protein Data Bank, Research Collaboratory for Structural Bioinformatics (RCSB).

* Corresponding author. Telephone: (515) 294-4971. Fax: (515) 294-0453. E-mail: hjfromm@iastate.edu.

[1] Abbreviations: FBPase, fructose-1,6-bisphosphatase; $F26P_2$, fructose 2,6-bisphosphate; $F16P_2$, fructose 1,6-bisphosphate; F6P, fructose 6-phosphate; P_i, inorganic phosphate; AMP, adenosine monophosphate; SDS−PAGE, sodium dodecyl sulfate−polyacrylamide gel electrophoresis; CD, circular dichroism.

10.1021/bi000609c CCC: $19.00
Published on Web 08/17/2000

steady-state fluorescence spectroscopy, to a variety of metal cations and physiologically relevant ligands

EXPERIMENTAL PROCEDURES

Materials. $F16P_2$, $F26P_2$, $NADP^+$, AMP, ampicillin, and IPTG were purchased from Sigma. DNA-modifying and restriction enzymes, T4 polynucleotide kinase, and ligase were from Promega. Glucose-6-phophate dehydrogenase and phosphoglucose isomerase were from Roche. Tryptone, yeast extract, and agar were from Difco. Other chemicals were reagent grade or the equivalent. *Escherichia coli* strains BMH 71-18 mutS and XL1-Blue came from Clontech and Stragene, respectively. FBPase-deficient strain DF 657 was from the Genetic Stock Center at Yale University.

Mutagenesis of FBPase. The mutation was introduced by changing specific bases in the double-stranded plasmid using the Transformer site-directed mutagenesis kit (*23*). The primer for the Tyr57 → Trp mutation was 5′-CGCAC-CTC**TGG**GGAATGG-3′ (codon for tryptophan underlined in boldface). The selection primer, 5′-CAGCCTCGC**CTC-GAG**AACGCCA-3′ (digestion site underlined in boldface), changed an original *Nru*I to a *Xho*I site on the plasmid. Unanticipated mutations were ruled out by sequencing the entire gene, after which the mutant plasmid was used in the transformation of *E. coli* DE 657 (DE3) cells. The Iowa State University sequencing facility provided DNA sequences, using the fluorescent dye dideoxy terminator method.

Expression and Purification of Wild-Type and Mutant FBPases. Expression and purification of FBPase were performed as previously described (*24*) with minor alterations. After cell breakage, the enzyme was concentrated by adding enough ammonium sulfate to produce a 70% saturated solution. The precipitate was then taken up in 20 mM Tris (pH 7.5) and desalted on a G-100 Sephadex column using the resuspension buffer. Fractions with FBPase activity were loaded onto a Cibacron Blue column and eluted with a NaCl gradient (0.5−1 M). FBPase appeared at approximately 0.8 M NaCl. The eluent was then dialyzed against 20 mM Tris-HCl (pH 8.3) and loaded onto a DEAE-Sephadex column and eluted with a NaCl gradient (from 0 to 0.3 M). FBPase appeared at a salt concentration of 0.15 M. The protein purity was determined by SDS−PAGE (12% gel) (*25*). The protein concentration was determined by the method of Bradford (*26*), using bovine serum albumin as a standard.

Kinetic Experiments. All assays employed the coupling of phosphoglucose isomerase and glucose-6-phosphate dehydrogenase (*1*). The specific activity, k_{cat}, and pH 7.5/pH 9.5 activity ratios were determined by directly monitoring the reduction of $NADP^+$ to NADPH at 340 nm. All other kinetic experiments monitored the fluorescence emission from NADPH at 470 nm, using an excitation wavelength of 340 nm (*7*). Initial rate data were analyzed using programs written either in MINITAB (*25*) or by ENZFITTER (*26*).

Circular Dichroism (CD) Spectroscopy. Spectra were recorded from 200 to 260 nm in steps of 1.3 nm on a Jasco J710 spectrometer in a 1 mm cell at room temperature using a protein concentration of approximately 0.25 mg/mL. Spectra were recorded in 20 mM Tris (pH 7.5) and with 20 mM Tris, 5 mM Mg^{2+}, 5 mM KP_i, and 5 mM F6P, with and without AMP (400 μM) or $F26P_2$ (240 μM). Each spectrum was blank-corrected and smoothed using the software provided with the instrument.

Crystallization of the Trp57 Mutant. Crystals of both T- and R-state product complexes grew from hanging drops with a total volume of 4 μL. T-State crystals grew from equal volumes of a protein solution [10 mg/mL Trp57 mutant, 100 mM Hepes (pH 7), 2 mM $ZnCl_2$, 5 mM F6P, 10 mM KP_i (pH 7), and 5 mM AMP] and a precipitant solution [100 mM Hepes (pH 7) and polyethylene glycol 3350 (17% w/v)]. R-State crystals grew from equal volumes of a protein solution, as above only without AMP, and a precipitant solution [100 mM Hepes (pH 7) and polyethylene glycol 3350 (6% w/v)]. Wells contained 500 μL of the precipitant solution. Crystals grew in approximately 2 days at 37 °C.

Data Collection. Data were collected from one T-state crystal (dimensions of 0.3 mm × 0.2 mm × 0.3 mm) and one R-state crystal (dimensions of 0.3 mm × 0.3 mm × 0.4 mm) at Iowa State University on a rotating anode/Siemens X-1000 area detector at 120 K, using Cu Kα radiation passed through a graphite monochromator. Data were reduced by XENGEN (*29*).

Model Refinement. Initial phases were calculated from the Zn^{2+}−product complex of wild-type FBPase (*18*) for the R-state structure and from the AMP−Zn^{2+}−product complex (*22*) for the T-state structure. Refinement employed XPLOR (*30*) as described previously (*19*). Constants of force and geometry for the protein came from Engh and Huber (*31*). In early rounds of refinement, models were heated to 2000 K and then cooled to 300 K in steps of 25 K. In later rounds of refinement, the systems were heated to 1000 K and cooled in steps of 10 K. After the slow cooling protocol was complete, the models were exposed to 120 steps of conjugated gradient minimization, followed by 20 steps of individual *B*-parameter refinement. Individual *B*-parameters were subject to the following restraints: nearest neighbor, main chain atoms, 1.5 Å^2; next-to-nearest neighbor, side chain atoms, 2.0 Å^2; nearest neighbor, side chain atoms, 2.0 Å^2; and next-to-nearest neighbor, side chain atoms, 2.5 Å^2. Water molecules were fit to difference electron density of 2.5σ or better and were added until no significant decrease was evident in R_{free}. For comparison of the mutant and wild-type structures, we employed programs from the CCp4 suite of programs (*32*).

Steady-State Fluorescence Measurements. Fluorescence data were collected using a SLM 8100C fluorimeter from Spectronic Instruments. To avoid exciting tyrosyl side chains, an excitation wavelength of 295 nm was used. Emission spectra were recorded in steps of 2 nm from 310 to 400 nm, using a slit width of 2 mm. Enzyme concentrations were from 0.2 to 0.5 μM. Each spectrum was an average of five to seven scans. Ligands were added to a solution of tryptophan (100 μM), to ascertain whether they alone influenced the fluorescence emission from tryptophan. Blanks were subtracted from all spectra, and corrections for protein dilutions were made. Conditions under which specific spectra were recorded are provided in the text, tables, and figure legends.

AMP titration data were analyzed by nonlinear least-squares fits, using the following equation:

$$\frac{\Delta F}{F_o} = \frac{(\Delta F_{max}/F_o)L^n}{K_d + L^n} \quad (1)$$

Table 1: Kinetic Parameters for Wild-Type and Tyr57 → Trp FBPases

	activity ratio (pH 7.5/pH 9.5)	k_{cat} (s^{-1})	K_m-F16P_2 (μM)	K_a-Mg^{2+} (mM^2)	Hill coefficient with Mg^{2+}	K_i-F26P_2 (μM)	I_{50}-AMP[a] (μM)	K^+ activation[b]
wild-type	3.3	22.0 ± 0.1	1.75 ± 0.08	0.67 ± 0.04	1.9 ± 0.1	0.264 ± 0.005	1.61 ± 0.05	16.8 ± 0.3
Trp57 mutant	3.3	24.0 ± 0.07	3.39 ± 0.09	0.53 ± 0.06	1.9 ± 0.1	0.84 ± 0.05	8.5 ± 0.4	16.6 ± 0.4

[a] The Hill coefficient of AMP inhibition is 2.0, as determined from a plot of Mg^{2+} concentration vs AMP concentration at a concentration of 20 μM F16P_2. [b] Percent increase in initial velocity in the presence of Mg^{2+} ($5K_a$) and F16P_2 ($5K_m$), caused by the addition of KCl (150 mM).

where ΔF is the change in fluorescence caused upon addition of ligand L, F_o is the fluorescence in the absence of ligand, K_d is the dissociation constant, and n is the Hill coefficient.

RESULTS

Kinetic Properties of Wild-Type FBPase and the Tyr57 → Trp Mutant. Wild-type and mutant proteins behave identically in chromatographic separations and are at least 95% pure, as determined by SDS−PAGE. The ratio of catalytic rates at pH 7.5 to 9.5 indicates an intact (nonproteolyzed) FBPase. The mutation of Tyr57 to tryptophan does not affect kinetic parameters significantly (Table 1). The K_i values for inhibition by AMP and F26P_2 increase 5- and 4-fold, respectively, relative to that of wild-type FBPase. Other mutations of loop 52−72 cause increases in K_i values for AMP and F26P_2 (*20*, *21*) and, along with the Trp57 mutant described here, may simply reflect the well-documented binding synergism of these ligands (*6*−*8*). Data from initial rate assays indicate no change in the mechanisms of inhibition by AMP and F26P_2.

Secondary Structure Analysis. The CD spectra of wild-type and Trp57 FBPases are identical from 200 to 260 nm (data not shown). CD spectra for the Trp57 mutant change in response to AMP, as noted in previous work on the wild-type enzyme (*15*). The Trp57 mutant also responds to the addition of F26P_2, yielding a CD spectrum that is identical to that observed in the presence of AMP.

Crystal Structures of R-State and T-State Trp57 FBPase. Crystals of the Trp57 mutant grown in the presence of Zn^{2+} and products (F6P and P_i) belong to space group $I222$ (a = 51.57 Å, b = 82.47 Å, and c = 165.57 Å) and are isomorphous with respect to the R-state, Zn^{2+}−product complex of the wild-type enzyme (*19*). Similarly, crystals of the Trp57 mutant grown in the presence of Zn^{2+}, products, and AMP belong to space group $P2_12_12$ (a = 59.82 Å, b = 165.48 Å, and c = 79.29 Å) and are isomorphous with respect to the T-state, Zn^{2+}−product−AMP complex of the wild-type enzyme (*22*). Statistics for data collection and refinement for both crystal forms are in Table 2. The stereochemistry of the models is generally very good as determined by PROCHECK (*33*). The method of Luzzati (*34*) indicates an uncertainty in coordinates of approximately 0.3 Å for both structures.

Residues 22−27, 142, and 143 are in weak electron density and have high thermal parameters in the R-state complex. The root-mean-square deviation between C^α atoms of the Trp57 mutant and wild-type FBPases is 0.28 Å for the entire model and 0.2 Å for loop 52−72. Deviations of up to 1.6 Å are in regions of weak electron density, as noted above. Distinct and strong electron density covers Trp57 and residues in its vicinity (Figure 1). The indole moiety of Trp57 occupies the same pocket as the side chain of Tyr57 of the wild-type enzyme, and is in contact with Ala51, Gly52, Leu126, Leu129, and Asp127 of its own subunit and Val196, Met172, and Met185 from the adjacent subunit (C1−C2 interface).

Table 2: Statistics of Data Collection and Refinement for Trp57 Complexes

	R-state	T-state
ligands bound	F6P, P_i, Zn^{2+}	F6P, P_i, Zn^{2+}, AMP
resolution (Å)	2.5	2.5
no. of measurements	38291	79656
no. of unique reflections	11308	25328
completeness of data (%)		
data set	88	90
last shell (2.7−2.5 Å)	74	83
R_{sym}[a]	5.00	6.86
no. of reflections in refinement[b]	9914	23834
no. of atoms	2646	5153
no. of solvent sites	111	175
R-factor[c]	0.178	0.192
R_{free}[d]	0.259	0.272
mean B ($Å^2$)	22	32
root-mean-square deviations		
bond lengths (Å)	0.009	0.008
bond angles (deg)	1.56	1.23
dihedral angles (deg)	24.7	24.8
improper dihedral angles (deg)	1.34	1.23

[a] $R_{sym} = \Sigma_j\Sigma_i|I_{ij} - \langle I_j\rangle|/\Sigma_i\Sigma_j I_{ij}$, where i runs over multiple observations of the same intensity and j runs over crystallographically unique intensities. [b] All data in the resolution range of 5−2.5 Å. [c] R-factor = $\Sigma||F_{obs}| - |F_{calc}||/\Sigma|F_{obs}|$, where $|F_{obs}| > 0$. [d] R-factor based upon 10% of the data randomly culled and not used in the refinement.

Residues 55−70, 142, 143, and 267−269 are in weak electron density in the T-state complex. Indeed, although residues 63−70 are part of the model, they are associated with electron density no higher than the noise level of the map. The root-mean-square deviation between C^α atoms of the mutant and wild-type structures is 0.39 Å over the entire model and 0.28 Å for residues 52−62 of the loop. Deviations of >1 Å appear among residues 63−70, 142, 143, and 267−269, because of absent or weak electron density. A modest level of electron density, however, covers Trp57 (Figure 2). In fact, the indole group of Trp57 occupies the same space as the side chain of Tyr57 in the wild-type T-state complex (*22*). The indole moiety of Trp57 is in contact with Ile53 and Ile56 of its own subunit and Val196, Ile10, and Ile194 of an adjacent subunit (C1−C2 interface). Trp57 is more exposed to solvent in the T-state (8.1 $Å^2$ accessible surface area to a 1.4 Å probe sphere) than in the R-state (6.4 $Å^2$ accessible surface area). Higher B-parameters in the T-state relative to those in the R-state suggest greater conformational mobility for Trp57 in the T-state structure. Indeed, position 57 is in proximity to residues 63−70, which are disordered completely and without electron density. The only difference between wild-type and Trp57 FBPases in the T-state concerns the binding of Zn^{2+}. In the wild-type structure, there is only one metal ion bound (at site 1), whereas in the mutant

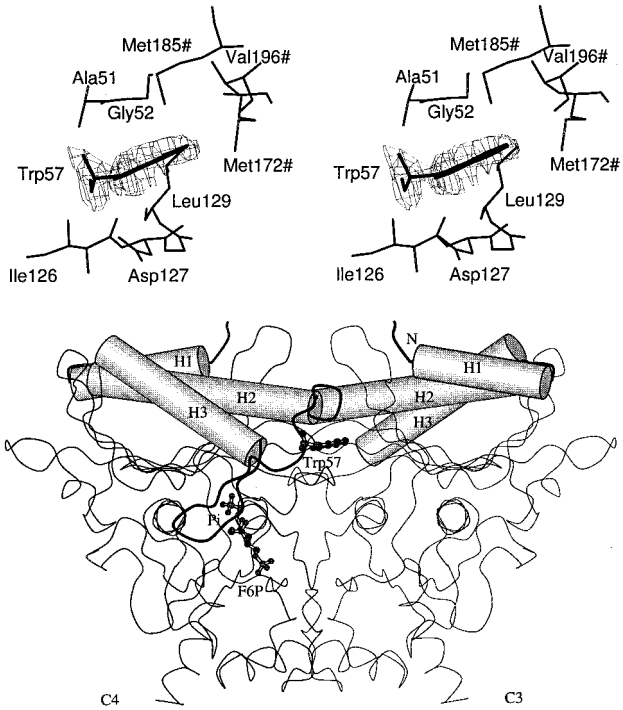

FIGURE 1: Structure of the Trp57 mutant in the R-state. Displayed is a stereoview of electron density from a $2F_{obs} - F_{calc}$ map associated with Trp57 at a contour level of 1σ (top) and an illustration of two subunits (labeled C3 and C4) of FBPase (bottom). Helices H1−H3 are represented as cylinders in both subunits, whereas loop 52−72 (engaged conformer, bold line) and Trp57, F6P, and P_i (ball-and-stick models) are presented only for subunit C4. The bottom image was drawn with MOLSCRIPT (*50*).

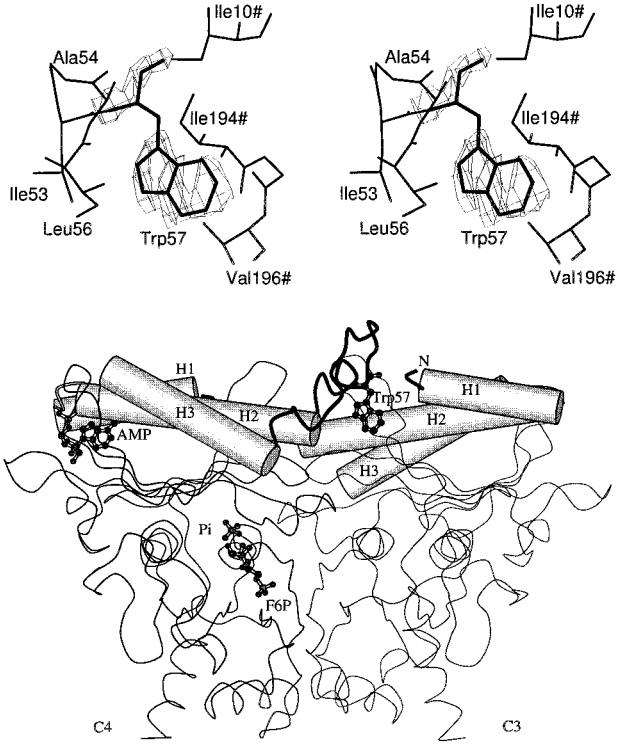

FIGURE 2: Structure of the Trp57 mutant in the T-state. Displayed is a stereoview of electron density from a $2F_{obs} - F_{calc}$ map associated with Trp57 at a contour level of 1σ (top) and an illustration of two subunits (labeled C3 and C4) of FBPase (bottom). Helices H1−H3 are represented as cylinders in both subunits, whereas loop 52−72 (disengaged conformer, bold line) and Trp57, F6P, P_i, and AMP (ball-and-stick models) are presented only for subunit C4. The bottom image was drawn with MOLSCRIPT (*50*).

structure, in addition to the metal at site 1, electron density appears at site 2, which is consistent with a Zn^{2+} cation at <40% occupancy or a water molecule.

Steady-State Fluorescence from the Trp57 Mutant. Ligands, alone or in combination, do not influence the fluorescence emission from a 100 μM tryptophan solution. In addition, the metal site proximal to Trp57 in the R- and T-states is 15 and 23 Å away, respectively. These distances exclude most quenching mechanisms except resonance energy transfer and electron transfer. Resonance energy transfer is not possible, simply because Mg^{2+}, Zn^{2+}, and Mn^{2+} do not absorb in the range of fluorescence emission from tryptophan. Electron transfer between the excited-state tryptophan and Mn^{2+} is possible, but is not reflected in the experimental data. The emission spectra of product complexes with Mn^{2+} and Zn^{2+} are equal in intensity, whereas that of Mg^{2+} is relatively low (see below). Electron transfer between Mn^{2+} and Trp57, however, should reduce the emission intensity from the Mn^{2+}−product complex relative to that from Mg^{2+} or Zn^{2+} complexes. Similarly, resonance energy transfer between bound AMP and Trp57 is not possible, because AMP does not absorb in the range of fluorescence emission of tryptophan. Recorded differences in fluorescence emission, then, must come from ligand-induced conformational changes, which alter the environment of Trp57.

All changes in fluorescence emission reported here are relative to the emission from the Trp57 mutant in the absence of ligands and divalent metal cations. The emission spectrum from the Trp57 mutant in the presence of Zn^{2+} (50 μM), F6P (5 mM), P_i (5 mM), and saturating AMP (400 μM) has a λ_{max} of 340 nm and a fluorescence intensity approximately equal to that of the ligand-free enzyme (Figure 3 and Table 3). In the absence of AMP, the level of fluorescence emission increases by 69% and λ_{max} shifts to 350 nm. The emission spectrum λ_{max} from the Trp57 mutant in the presence of $F26P_2$ (240 μM), with or without Zn^{2+}, F6P, and P_i, is 15% higher than that from the Zn^{2+}−product−AMP complex, with a λ_{max} of 342 nm. The addition of $F26P_2$ to the Zn^{2+}−product−AMP complex, however, causes no detectable change in fluorescence emission (data not shown).

The emission spectra in the presence of F6P (5 mM), P_i (5 mM), and AMP (400 μM) with Mg^{2+} (5 mM) or Mn^{2+} (0.5 mM) are identical to that of the Zn^{2+}−product−AMP complex (Figure 3 and Table 3). In the absence of AMP and in the presence of products, however, Mg^{2+} causes a much smaller increase in the level of fluorescence emission (23%) and a smaller shift in λ_{max} to 346 nm than does either Zn^{2+} or Mn^{2+}. The addition of K^+ (as KCl), at levels (150 mM) sufficient to saturate the monovalent cation site, caused no change in fluorescence emission. The emission spectrum in the presence of products, $F26P_2$ and Mg^{2+}, however, is nearly identical to that of the corresponding complex with Zn^{2+}. The level of fluorescence emission from the Trp57 mutant in the presence of products, $F26P_2$ and Mn^{2+}, is 46% higher than that of the metal−product−AMP complexes, compared to 15% and 11% increases, respectively, when Zn^{2+} and Mg^{2+} are used.

The change in fluorescence from the Zn^{2+}−product complex in response to the titration of AMP establishes a K_d for AMP of 16 μM and a Hill coefficient of 2.1 (Figure 4). These values are very close to the I_{50}-AMP (22 μM) and

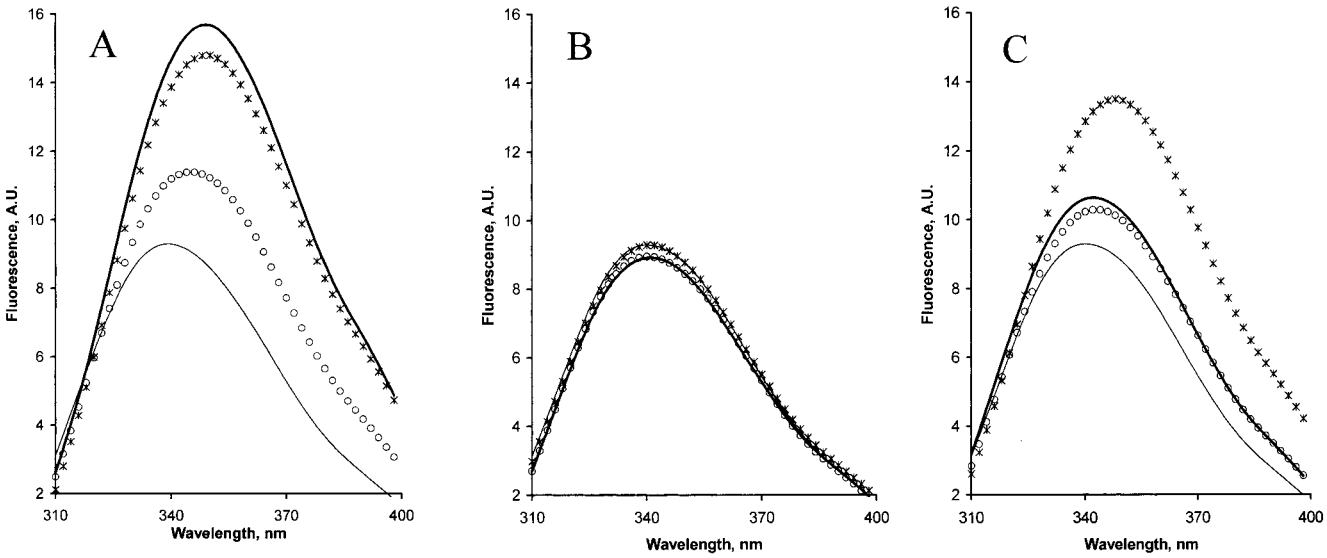

FIGURE 3: Fluorescence spectra of the Trp57 mutant under different ligation conditions. (A) Enzyme under R-state conditions of ligation (5 mM F6P and 5 mM KP_i) in the presence of 50 μM Zn^{2+} (bold line), 0.5 mM Mn^{2+} (asterisks), 5 mM Mg^{2+} (open circles), and no metal (solid line). (B) Enzyme under T-state conditions of ligation (5 mM F6P, 5 mM KP_i, and 0.4 mM AMP) in the presence of 50 μM Zn^{2+} (bold line), 0.5 mM Mn^{2+} (asterisks), 5 mM Mg^{2+} (open circles), and no metal (solid line). (C) Enzyme in the presence of F26P2 (240 μM) and products (5 mM F6P and 5 mM KP_i) in the presence of 50 μM Zn^{2+} (bold line), 0.5 mM Mn^{2+} (asterisks), 5 mM Mg^{2+} (open circles), and no metal (solid line).

Table 3: Fluorescence Emission from Ligated Complexes of Trp57 FBPase

	5 mM F6P and KP_i		5 mM F6P and KP_i with 400 μM AMP		5 mM F6P and KP_i with 240 μM $F26P_2$	
divalent cation	F^a	λ_{max} (nm)	F^a	λ_{max} (nm)	F^a	λ_{max} (nm)
none	1.00	340	1.00	340	1.00	340
Zn^{2+} (50 μM)	1.69	350	0.96	340	1.15	342
Mg^{2+} (5 mM)	1.23	346	0.96	342	1.11	340
Mn^{2+} (0.5 mM)	1.59	350	1.00	340	1.46	348

[a] Relative fluorescence emission at λ_{max} from the Trp57 mutant without divalent cations in the presence of F6P (5 mM) and KP_i (5 mM).

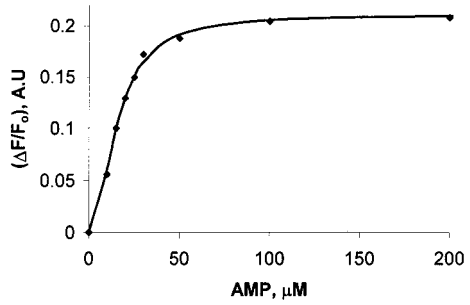

FIGURE 4: AMP titration of the Trp57 mutant as monitored by fluorescence emission. The enzyme is in 5 mM F6P, 5 mM P_i, and 50 μM Zn^{2+}. AMP is added up to a final concentration of 0.2 mM.

Hill coefficient (2.0) determined by kinetics at saturating Mg^{2+} concentrations (5 mM).

DISCUSSION

The mutation of Tyr57 to tryptophan results in only minor changes in the functional and structural properties of FBPase. Crystal structures of the Zn^{2+}−product complex of the Trp57 mutant in the presence and absence of AMP are virtually identical to those of the wild-type enzyme under the same crystallization conditions. Using Mg^{2+} as the cation activator, many of the functional properties of FBPase (pH 7.5/pH 9.5 activity ratio, k_{cat}, K_m for $F16P_2$, potassium activation, and Hill coefficients for Mg^{2+} and AMP) are indistinguishable from those of the wild-type enzyme. The 4- and 5-fold increases in K_i values for $F26P_2$ and AMP, respectively, do indicate a mutation-dependent change in functional properties; however, the elevated K_i values probably result from the enhanced stability of the R-state relative to the T-state of the mutant. Elevated K_i values for both AMP and $F26P_2$ are consistent with the model of Choe et al. (*19*), which requires AMP-bound and $F26P_2$-bound states of FBPase to have disengaged loops. Any mutation, which stabilizes an engaged loop 52−72, should increase the K_i values of AMP and $F26P_2$. Under extremes in ligand concentration (AMP absent and AMP saturating) and the presence of Zn^{2+}−product complexes, the Trp57 mutant adopts the R- and T-state conformations of the wild-type enzyme. Furthermore, initial velocity assays indicate no change in the kinetic mechanisms of inhibition by AMP (competitive with respect to Mg^{2+} and noncompetitive with respect to $F26P_2$) and $F26P_2$ (competitive with respect to $F16P_2$). Evidently, tryptophan at position 57 is a nonperturbing spectroscopic probe of enzyme function and conformation.

Common quenchers of tryptophan fluorescence are water, the peptide bond, and specific amino acid side chains (*35*). The indole group of Trp57 in the T-state is neither close to a side chain particularly effective as a quencher, nor does its exposure to solvent differ significantly from that in the R-state (8.1 vs 6.4 Å^2). FBPase, however, is not a static structure. Thermal parameters are an approximate measure of conformational dynamics, and on the basis of such parameters, the indole of Trp57 undergoes greater conformational movement in the T-state than in the R-state. We may observe electron density for only the most solvent inaccessible conformer for Trp57 in the T-state. Other conformers would convolute the electron density of Trp57 with that of the solvent, resulting in a uniform carpet of electron density, indistinguishable from noise. The wave-

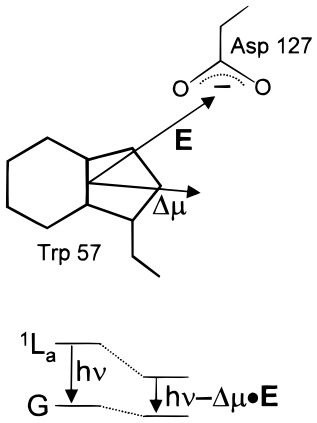

FIGURE 5: Schematic of the electrostatic perturbation due to Asp127 on the fluorescence emission energy from Trp57. The difference dipole moment $\Delta\mu$ is the dipole moment of ground-state indole subtracted from the dipole moment of the ^1L_a excited state. Its orientation here is based on information provided by Callis (*51*). The change in energy between ground and excited states due to a point negative charge positioned between the oxygen atoms of the side chain of Asp127 is $-\Delta\mu \times E$. Given the geometrical relationship of Asp127 to Trp57, the electrostatic perturbation decreases the separation in ground state and ^1L_a energy levels, causing a red shift in the fluorescence emission.

length of maximum fluorescence emission for tryptophan (λ_{max}) in water is 352 nm and decreases in more hydrophobic environments (*36*). The observed λ_{max} for Trp57 in the T-state is approximately 340 nm, which is consistent with a mixture of solvent-exposed and hydrophobic environments for the indole group.

Trp57 in the R-state occupies a pocket lined primarily with hydrophobic side chains. The thermal parameters for the indole moiety in the R-state reflect a fully occupied conformational state, with moderate conformational movement. The λ_{max} for an indole under such circumstances should be blue-shifted relative to tryptophan in solution, but λ_{max} occurs at approximately 350 nm. This anomalous behavior of the indole group in the R-state may arise from its specific electrostatic environment, which may be dominated by the negative charge of Asp127 (Figures 1 and 5). The difference dipole vector, determined from the dipole moments of the ground and excited (^1L_a) states of indole, lies in the plane of the fused ring and is directed approximately as shown in Figure 5. The electrostatic field caused by Asp127 will decrease the energy separation between the ground and excited states. That decrease is consistent with the 10 nm red shift in the R-state spectrum relative to the T-state spectrum.

The environment of Trp57 in the R-state may influence fluorescence emission by other mechanisms as well. Although the imino group of the indole ring does not make a hydrogen bond in the crystal structure, backbone carbonyl 126 and the side chain of Asp127 need move by no more than 1 Å to hydrogen bond with the indole group. Hydrogen bonding with the indole would contribute to the observed red shift, noted above. Additionally, several surrounding side chains are effective quenchers of fluorescence (*35*). Asp127, His253, Cys183, and Tyr258 are 3.4, 6.8, 7.1, and 7.5 Å, respectively, from the indole moiety in the R-state. In the absence of one or several of these side chains, the level of fluorescence emission from Trp57 could increase significantly.

A two-state system (disengaged loop, T-state and engaged loop, R-state) cannot account for the variation in fluorescence spectra observed in the study presented here. First, the Trp57 mutant, in the absence of metal activators and other ligands, has a disengaged loop, as evidenced by its low level of fluorescence emission. In fact, the fluorescence spectrum in the absence of all ligands is nearly indistinguishable from spectra of metal−product−AMP complexes (Figure 3). On the basis of CD spectroscopy, however, the Trp57 mutant, in the absence of ligands, is in the R-state. Evidently, the fluorescence spectrum of the Trp57 mutant is not sensitive to the quaternary conformation of FBPase (T- or R-state), as is CD spectroscopy, but is instead sensitive to the conformational state of loop 52−72 (engaged or disengaged). Work of Lipscomb and colleagues has revealed R-state, disengaged loop conformers of wild-type FBPase under a number of crystallization conditions (*37*−*39*). Hence, an R-state, disengaged loop conformer for FBPase is probably a well-populated state for the enzyme in solution.

Variations in fluorescence emission levels of metal−product complexes could reflect differences in the equilibrium populations of R-state conformers (engaged vs disengaged loop). If so, then Mg^{2+} would be the least effective of the divalent cations in stabilizing the R-state, engaged conformation of FBPase. Indeed, of the divalent cation activators, Mg^{2+} binds to FBPase with much lower affinity than either Mn^{2+} or Zn^{2+}, and its level of fluorescence emission is significantly lower than that of Mn^{2+} or Zn^{2+}.

Although attractive for its simplicity, the above explanation for the low level of fluorescence emission from the Mg^{2+}−product complex is difficult to reconcile with the absence of a K^+-induced increase in the level of fluorescence emission. K^+ putatively binds to or near metal site 3, which is unoccupied by Mg^{2+} at a concentration of 5 mM (*22*). Directed mutations of loop residues, which weaken Mg^{2+} association, also abolish K^+ activation (*21*). Hence, if the low level of fluorescence emission observed from the Mg^{2+}−product complex is due to an equilibrium mixture of engaged and disengaged conformers, then the addition of K^+ should stabilize the engaged loop and thereby enhance fluorescence emission. Such is not the case. Evidently, if K^+ does bind to metal site 3, it does not influence the time-averaged environment of Trp57. The low level of fluorescence emission from the Mg^{2+}−product complex then may reflect a different conformational state for FBPase (see below).

On the basis of difference spectroscopy, AMP and $F26P_2$ stabilize the same conformation of FBPase (*40*), presumably a T-state, disengaged loop conformation. Fluorescence emission spectra from the Trp57 mutant in the presence of saturating $F26P_2$ or saturating AMP, however, are not identical. The time-averaged environment of Trp57 is probably less solvent accessible in metal−$F26P_2$ complexes, than in metal−AMP complexes. Conceivably, metal−$F26P_2$ complexes may be an equilibrium mixture of loop-engaged and disengaged conformers. If so, then Mn^{2+} must stabilize more of the metal−$F26P_2$ complex in the engaged loop conformation, than either Zn^{2+} or Mg^{2+}. Indeed, $F26P_2$ is almost 50-fold less effective as an inhibitor of FBPase when assayed with Mn^{2+} than with either Mg^{2+} or Zn^{2+} (*41*). Alternatively, the conformation of metal−$F26P_2$ complexes of the Trp57 mutant may represent distinct conformational states of loop 52−72, rather than an equilibrium mixture of

engaged and disengaged loops. Available crystal structures of $F26P_2$ complexes of FBPase may not be faithful representations of metal−$F26P_2$ complexes, because of the degradation of $F26P_2$ to F6P on one hand (*42*, *43*) and the inclusion of AMP on the other (*17*, *44*). As the emission spectra of metal−product−$F26P_2$−AMP and metal−product−AMP complexes are identical, AMP evidently stabilizes the same T-state, disengaged loop conformation to the exclusion of all other conformers.

Fluorescence spectra of the Trp57 mutant are clearly consistent with a dynamic loop, sensitive to cation activators and specific ligands. The crystallographic structures (R-state, engaged loop; R-state, disengaged loop; and T-state, disengaged loop), however, may represent only some of the well-populated conformational states of FBPase in solution. Cation-dependent differences in fluorescence emission from the Trp57 mutant are real and are in harmony with reports of differing kinetic mechanisms and anomeric specificity with Mg^{2+} and Mn^{2+} (*1*, *45*−*47*). As a consequence of the symmetry inherent in crystal structures, FBPase has been represented in solution as a tetramer, which retains three intersecting axes of symmetry. Reports are in the literature, however, regarding half-of-sites reactivity and pairwise association of AMP (*48*, *49*), which necessarily requires the loss of at least one symmetry axis of the tetramer. These asymmetric conformers of FBPase may account for the variety of conformational states inferred by fluorescence spectroscopy.

REFERENCES

1. Benkovic, S. T., and de Maine, M. M. (1982) *Adv. Enzymol. Relat. Areas Mol. Biol. 53*, 45−82.
2. Tejwani, G. A. (1983) *Adv. Enzymol. Relat. Areas Mol. Biol. 54*, 121−194.
3. Van Schagtingen, E., and Hers, H. G. (1981) *Proc. Natl. Acad. Sci. U.S.A. 78*, 2861−2863.
4. Pilkis, S. J., El-Maghrabi, M. R., and Claus, T. H. (1988) *Annu. Rev. Biochem. 57*, 755−783.
5. Pilkis, S. J., El-Maghrabi, M. R., and Claus, T. H. (1981) *J. Biol. Chem. 256*, 3619−3622.
6. Scheffler, J. E., and Fromm, H. J. (1986) *Biochemistry 25*, 6659−6665.
7. Liu, F., and Fromm, H. J. (1990) *J. Biol. Chem. 265*, 7401−7406.
8. Nimmo, H. G., and Tipton, K. F. (1975) *Eur. J. Biochem. 58*, 567−574.
9. Liu, F., and Fromm, H. J. (1988) *J. Biol. Chem. 263*, 9122−9128.
10. Stone, S. R., and Fromm, H. J. (1980) *Biochemistry 19*, 620−625.
11. Ke, H., Zhang, Y., Liang, J.-Y., and Lipscomb, W. N. (1991) *Proc. Natl. Acad. Sci. U.S.A. 88*, 2989−2993.
12. Liu, F., and Fromm, H. J. (1988) *J. Biol. Chem. 19*, 9122−9128.
13. Marcus, F., Edelstein, I., Reardon, I., and Heinrikson, R. L. (1982) *Proc. Natl. Acad. Sci. U.S.A. 79*, 7161−7165.
14. Zhang, Y., Liang, J.-Y., Huang, S., and Lipscomb, W. N. (1994) *J. Mol. Biol. 244*, 609−624.
15. Shyur, L.-F., Aleshin, A. E., Honzatko, R. B., and Fromm, H. J. (1996) *J. Biol. Chem. 271*, 33301−33307.
16. Ke, H., Zhang, Y., Liang, J.-Y., and Lipscomb, W. N. (1990) *Proc. Natl. Acad. Sci. U.S.A. 87*, 5243−5247.
17. Xue, Y., Huang, S., Liang, J.-Y., Zhang, Y., and Lipscomb, W. N. (1994) *Proc. Natl. Acad. Sci. U.S.A. 26*, 12482−12486.
18. Villeret, V., Huang, S., Zhang, Y., and Lipscomb, W. N. (1995) *Biochemistry 34*, 4307−4315.
19. Choe, J.-Y., Poland, B. W., Fromm, H. J., and Honzatko, R. B. (1998) *Biochemistry 37*, 11441−11450.
20. Kurbanov, F. T., Choe, J.-Y., Honzatko, R. B., and Fromm, H. J. (1998) *J. Biol. Chem. 273*, 17511−17516.
21. Nelson, S. W., Choe, J.-Y., Honzatko, R. B., and Fromm, H. J. (2000) *J. Biol. Chem.* (in press).
22. Choe, J.-Y., Fromm, H. J., and Honzatko, R. B. (2000) *Biochemistry 39*, 8565−8574.
23. Deng, W. P., and Nickoloff, J. A. (1992) *Anal. Biochem. 200*, 81−88.
24. Burton, V. A., Chen, M., Ong, W.-C., Ling, T., and Fromm, H. J. (1993) *Biochem. Biophys. Res. Commun. 192*, 511−517.
25. Laemmli, U. K. (1970) *Nature 227*, 680−685.
26. Bradford, M. M. (1976) *Anal. Biochem. 72*, 248−252.
27. Siano, D. B., Zyskind, J. W., and Fromm, H. J. (1975) *Arch. Biochem. Biophys. 319*, 587−600.
28. Leatherbarrow, R. J. (1987) *ENZFITTER: A Non-Linear Regression Data Analysis Program for the IBM PC*, pp 13−75, Elsevier Science Publishers, Amsterdam.
29. Howard, A. J., Nielsen, C., and Xuong, N. H. (1985) *Methods Enzymol. 114*, 452−472.
30. Brünger, A. T. (1992) *XPLOR*, version 3.1, Yale University Press, New Haven, CT.
31. Engh, R. A., and Huber, R. (1991) *Acta Crystallogr. A47*, 392−400.
32. Otwinowski, Z. (1993) *Proceedings of the CCP4 study weekend: data collection and processing* (Sawyer, L., Isaacs, N., and Bailey, S., Eds.) pp 56−62, SERC Daresbury Laboratory, Warrington, England.
33. Laskowski, R. A., MacArthur, M. W., Moss, D. S., and Thorton, J. M. (1993) *J. Appl. Crystallogr. 26*, 283−291.
34. Luzzati, V. (1956) *Acta Crystallogr. 5*, 802−810.
35. Chen, Y., and Barkley, M. D. (1998) *Biochemistry 37*, 9976−9982.
36. Lakowicz, J. R. (1999) *Principles of Fluorescence Spectroscopy*, 2nd ed., pp 185−193, Kluwer Academic/Plenum Publishers, New York.
37. Zhang, Y., Liang, J. Y., Huang, S., Ke, H., and Lipscomb, W. N. (1993) *Biochemistry 32*, 1844−1857.
38. Ke, H. M., Liang, J. Y., Zhang, Y., and Lipscomb, W. N. (1991) *Biochem. J. 86*, 4412−4420.
39. Ke, H. M., Thorpe, C. M., Seaton, B. A., Marcus, F., and Lipscomb, W. N. (1989) *Proc. Natl. Acad. Sci. U.S.A. 86*, 1475−1479.
40. McGrane, M. M., El-Maghrabi, M. R., and Pilkis, S. J. (1983) *J. Biol. Chem. 258*, 10445−10454.
41. Mizunuma, H., and Tashima, Y. (1983) *Arch. Biochem. Biophys. 226*, 257−264.
42. Ke, H. M., Thorpe, C. M., Seaton, B. A., Lipscomb, W. N., and Marcus, F. (1990) *J. Mol. Biol. 3*, 513−539.
43. Liang, J.-Y., Huang, S., Zhang, Y., Ke, H., and Lipscomb, W. N. (1992) *Proc. Natl. Acad. Sci. U.S.A. 6*, 2404−2408.
44. Ke, H., Zhang, Y., and Lipscomb, W. N. (1990) *Proc. Natl. Acad. Sci. U.S.A. 87*, 5243−5247.
45. Frey, W., Fishbein, R., de Maine, M. M., and Benkovic, S. J. (1977) *Biochemistry 16*, 2479−2484.
46. Benkovic, P. A., Bullard, W. P., de Maine, M. M., Fishbein, R., Schray, K. J., Steffens, J. J., and Benkovic, S. J. (1974) *J. Biol. Chem. 249*, 930−931.
47. Domanico, P. L., Rahil, J. F., and Benkovic, S. J. (1985) *Biochemistry 24*, 1623−1628.
48. Lu, G., Stec, B., Giroux, E. L., and Kantrowitz, E. R. (1996) *Protein Sci. 11*, 2333−2342.
49. Rahil, J. F., de Maine, M. M., and Benkovic, S. J. (1982) *Biochemistry 21*, 3358−3363.
50. Kraulis, J. (1991) *J. Appl. Crystallogr. 24*, 946−950.
51. Callis, P. R. (1997) *Methods Enzymol. 278*, 113−150.

BI000609C